Available online at www.sciencedirect.com
SCIENCE DIRECT®
Journal of Magnetic Resonance 159 (2002) 25–35
JMR Journal of Magnetic Resonance
www.academicpress.com

Double-quantum solid-state NMR of ^{13}C spin pairs coupled to ^{14}N

C.E. Hughes,[a,1] R. Pratima,[a] T. Karlsson,[a,2] and M.H. Levitt[a,b,*]

[a] *Physical Chemistry Division, Arrhenius Laboratory, Stockholm University, 106 91 Stockholm, Sweden*
[b] *Department of Chemistry, University of Southampton, Southampton SO17 1BJ, UK*

Received 8 March 2002; revised 30 July 2002

Abstract

We examine the double-quantum magic angle spinning NMR spectra of pairs of ^{13}C nuclei coupled to one or more ^{14}N nuclei. The experimental spectra of $^{13}C_2$-glycine and glycyl-[$^{13}C_2$]-glycyl-glycine are used to demonstrate the sensitivity of the spectra to the orientation of ^{14}N quadrupole interaction tensors and to the molecular torsional angles.

Keywords: ^{14}N quadrupole; Solid-state NMR; Double-quantum NMR; Magic-angle spinning; Torsional angles

1. Introduction

Magic-angle spinning (MAS) is widely used for obtaining well-resolved spectra of dilute spin species in powdered solids. The spectral narrowing achieved by MAS is due to the averaging out of anisotropic second-rank spin interactions such as the dipole–dipole couplings and the chemical shift anisotropies. In most circumstances, routinely available MAS frequencies of tens of kHz are sufficient to obtain narrow spectral peaks from dilute spin species such as ^{13}C in the presence of a strong proton decoupling field.

The situation is more complicated if one or more of the spin sites has an additional interaction which does not commute with the dipole–dipole coupling and which is comparable in magnitude to the Zeeman interaction with the static magnetic field. The most common case is when one or more spins have a significant electric quadrupole interaction. For example, the MAS spectra of ^{13}C sites coupled to ^{14}N spins ($I = 1$) often display an asymmetric doublet structure which is due to the interaction of the large ^{14}N quadrupolar coupling and the ^{14}N–^{13}C dipole–dipole coupling [1–3]. This residual dipolar splitting is inversely proportional to the applied magnetic field. The residual splitting structure may be analysed to estimate the quadrupolar interaction parameters of the ^{14}N site and the relative orientations of the quadrupolar and dipolar interaction tensors [4].

In this paper, we investigate the double-quantum spectra of ^{13}C pairs coupled to one or more ^{14}N spins. This study falls within the scope of double-quantum heteronuclear local field spectroscopy (2Q-HLF) [5–12] which has been used to estimate molecular geometric parameters such as torsional angles. In such experiments, double-quantum coherence between pairs of ^{13}C spins is excited and allowed to evolve under the influence of coupling to neighbouring heteronuclei. The first 2Q-HLF experiment developed was HCCH-2Q-HLF [5], in which $^{13}C_2$ double-quantum coherence evolved under the ^{1}H–^{13}C interactions, the homonuclear ^{1}H–^{1}H interactions being removed by the application of a homonuclear decoupling pulse sequence to the ^{1}H nuclei. The method was applied to carbohydrates [6,7] and to retinal membrane proteins [8–10]. The NCCN-2Q-HLF experiment [11,12] was also developed and applied to samples which were labelled with ^{15}N as well as ^{13}C. In this case, the small ^{15}N–^{13}C dipolar interactions were recoupled by a suitable RF pulse sequence during the

* Corresponding author. Tel.: +44-23-8059-3781; fax: +44-23-8059-6753.
E-mail address: mhl@soton.ac.uk (M.H. Levitt).
[1] Present address: Max Planck Institute for Biophysical Chemistry, 37077 Göttingen, Germany.
[2] Present address: Department of Chemistry, University of Washington, Seattle, WA 98195, USA.

1090-7807/02/$ - see front matter
PII: S1090-7807(02)00118-0

$^{13}C_2$ double-quantum evolution. The HCCH-2Q-HLF and NCCN-2Q-HLF experiments were both used to measure torsional angles since the double-quantum ^{13}C spectra are dependent upon the relative orientations of the ^{1}H–^{13}C and ^{15}N–^{13}C vectors.

In this paper, we discuss the application of $^{13}C_2$ double-quantum spectroscopy to samples containing naturally abundant ^{14}N nuclei, rather than samples labelled with ^{15}N. In the case of ^{14}N, there is often no need to actively recouple the ^{14}N nuclei to the ^{13}C spins by using RF fields, since the large quadrupole couplings of the ^{14}N spins accomplish a partial recoupling themselves without outside intervention. The double-quantum spectra of ^{13}C pairs coupled to one or more ^{14}N spins display a complicated residual coupling structure which is sensitive to the molecular geometry and to the orientation of the ^{14}N electric quadrupole interactions.

In the discussion below, we describe experiments in which the ^{13}C pair is coupled to a single ^{14}N spin (called ^{14}NCC-2Q-HLF) and experiments in which the ^{13}C pair is coupled to two ^{14}N spin (called ^{14}NCC^{14}N-2Q-HLF). The two experiments differ only in the sample used. The basic experimental technique for the two is exactly the same.

One of the most important opportunities of NCCN torsional angle experiments is in the MAS NMR of [^{13}C, ^{15}N]-labelled peptides and proteins [11,12]. The evolution of the double-quantum coherence involving the $^{13}C^{\alpha}$ site and the neighbouring $^{13}C'$ site is sensitive to the relative orientation of the ^{15}N–$^{13}C^{\alpha}$ and $^{13}C'$–^{15}N dipole–dipole couplings and, hence, to the backbone torsional angle, ψ (Fig. 1a). The NCCN experiment involving ^{15}N labels is not sensitive to the torsional angle ϕ, since this angle describes the rotation about the ^{15}N–$^{13}C'$ bond and does not modulate the relative orientation of the two ^{13}C–^{15}N vectors. By contrast, the ^{14}NCC^{14}N-2Q-HLF experiment is sensitive to both the angles ϕ and ψ. This is because it is dependent upon the orientation of the electric field gradient at the ^{14}N site which is, in turn, dependent upon the local environment of the nitrogen. The ^{14}NCC^{14}N-2Q-HLF experiment therefore has a potentially higher information content than the ^{15}NCC^{15}N-2Q-HLF experiment. In some cases, the use of naturally abundant ^{14}N spins rather than the enriched ^{15}N isotope may also have advantages of cost and convenience.

In this paper, we investigate the ^{1}H-decoupled evolution of $^{13}C_2$ double-quantum coherence in two model samples: [$^{13}C_2$]-glycine, in which the two ^{13}C nuclei have a significant dipole–dipole coupling with the ^{14}N site, and glycyl-[$^{13}C_2$]-glycyl-glycine, which contains the ^{14}N–^{13}C–^{13}C–^{14}N moiety typical of peptides and proteins. We examine the structure of the $^{13}C_2$ double-quantum spectra and assess their information content, with respect to the orientation of the interaction tensors orientations and the molecular torsional angles.

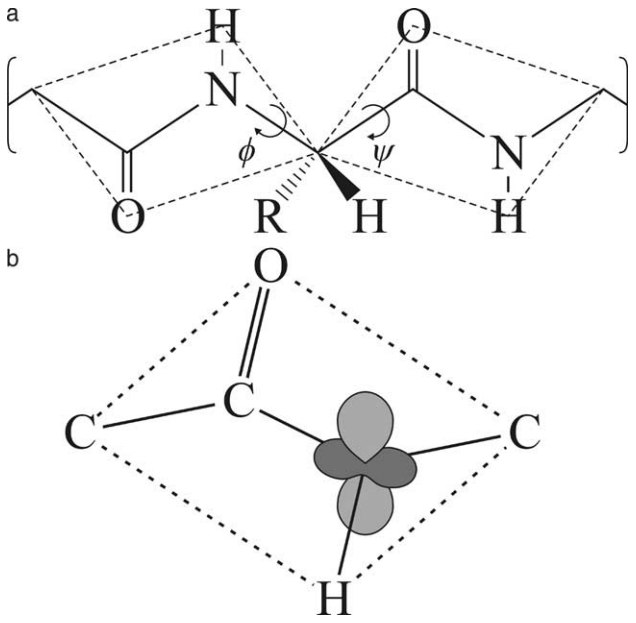

Fig. 1. (a) Backbone conformation of an amino acid within a peptide chain, showing the Ramachandran torsional angles ϕ and ψ. Dotted lines indicate the planes of the two peptide bonds. (b) Standard orientations for the ^{14}N electric field gradient in a peptide bond assumed to be planar. The largest component (V_{zz}) is perpendicular to the peptide plane. The smallest component (V_{yy}) is along the N–H bond. The two shades of grey indicate regions of opposite sign of the EFG.

2. Theory

2.1. One ^{13}C coupled to one ^{14}N

The calculation of the MAS ^{13}C spectrum in a ^{13}C–^{14}N system has been presented in several different ways [4,13–15]. It is summarized below to establish the notation and to emphasize the dependence upon the molecular geometry and quadrupole interaction parameters.

The Hamiltonian for coupled $I = 1$ and $I = 1/2$ nuclei is given by

$$\mathscr{H} = \mathscr{H}_{Z} + \mathscr{H}_{CS} + \mathscr{H}_{J} + \mathscr{H}_{D} + \mathscr{H}_{Q}, \tag{1}$$

where $\mathscr{H}_{Z}$, $\mathscr{H}_{CS}$, and $\mathscr{H}_{J}$ are the Zeeman, chemical shift, and J-coupling Hamiltonians. $\mathscr{H}_{D}$ and $\mathscr{H}_{Q}$ are the heteronuclear dipole–dipole and quadrupolar interaction Hamiltonians, given by

$$\begin{aligned} \mathscr{H}_{D} &= \sum_{n} (-1)^{n} [A^{D}_{2,n}]^{F} [T^{D}_{2,-n}]^{F}, \\ \mathscr{H}_{Q} &= \sum_{n} (-1)^{n} [A^{Q}_{2,n}]^{F} [T^{Q}_{2,-n}]^{F}, \end{aligned} \tag{2}$$

where $T^{D}_{2,-n}$ and $T^{Q}_{2,-n}$ are the irreducible spherical tensor spin operators for the dipole and quadrupole interactions expressed in an arbitrary reference frame, F. These tensor components are defined elsewhere [16]. The spatial components of the irreducible spherical tensors in the laboratory frame, $[A^{D}_{2,n}]^{L}$ and $[A^{Q}_{2,n}]^{L}$, are given by

$$[A^{\mathrm{D}}_{2,n}]^{\mathrm{L}} = \sum_m [A^{\mathrm{D}}_{2,m}]^{\mathrm{P}} D^2_{m,n}(\Omega^{\mathrm{D}}_{\mathrm{PL}}),$$
$$[A^{\mathrm{Q}}_{2,n}]^{\mathrm{L}} = \sum_m [A^{\mathrm{Q}}_{2,m}]^{\mathrm{P}} D^2_{m,n}(\Omega^{\mathrm{Q}}_{\mathrm{PL}}), \tag{3}$$

where the principal axis components, $[A^{\mathrm{D}}_{2,n}]^{\mathrm{P}}$ and $[A^{\mathrm{Q}}_{2,n}]^{\mathrm{P}}$, are given by

$$[A^{\mathrm{D}}_{2,0}]^{\mathrm{P}} = -\sqrt{6}\frac{\mu_0\gamma_{\mathrm{N}}\gamma_{\mathrm{C}}\hbar}{4\pi r^3_{ij}}, \quad [A^{\mathrm{D}}_{2,\pm1}]^{\mathrm{P}} = [A^{\mathrm{D}}_{2,\pm2}]^{\mathrm{P}} = 0,$$
$$[A^{\mathrm{Q}}_{2,0}]^{\mathrm{P}} = 2\pi\sqrt{3/8}C_{\mathrm{Q}}, \quad [A^{\mathrm{Q}}_{2,\pm1}]^{\mathrm{P}} = 0, \tag{4}$$
$$[A^{\mathrm{Q}}_{2,\pm2}]^{\mathrm{P}} = -2\pi\eta C/4.$$

Here $\Omega^{\mathrm{D}}_{\mathrm{PL}} = \{\alpha^{\mathrm{D}}_{\mathrm{PL}}, \beta^{\mathrm{D}}_{\mathrm{PL}}, \gamma^{\mathrm{D}}_{\mathrm{PL}}\}$ and $\Omega^{\mathrm{Q}}_{\mathrm{PL}} = \{\alpha^{\mathrm{Q}}_{\mathrm{PL}}, \beta^{\mathrm{Q}}_{\mathrm{PL}}, \gamma^{\mathrm{Q}}_{\mathrm{PL}}\}$ are the Euler angles relating the principal axis systems of the dipole and quadrupole interactions to the laboratory frame, which is defined such that the z-axis is along the static field. In this paper, the quadrupole interaction is defined such that $C_{\mathrm{Q}} = eQV_{zz}/h$, where Q is the nuclear electric quadrupole moment and e is the proton charge. As in [17], the principal values of the electric field gradient (EFG) tensor are ordered such that

$$|V_{zz}| \geqslant |V_{xx}| \geqslant |V_{yy}|. \tag{5}$$

The asymmetry parameter of the quadrupolar interaction is defined as $\eta = (V_{yy} - V_{xx})/V_{zz}$. The relationship between the reference frames is sketched in Fig. 2a.

In a ^{13}C–^{14}N system, the ^{13}C spectrum is generated by the three (−1)-quantum coherences, denoted here as Liouville kets [18,19] $\{|+1,-),|0,-),|-1,-)\}$, and defined through

$$|n,-) = |n,-1/2\rangle\langle n,+1/2|, \tag{6}$$

where $|n,m\rangle$ is a perturbed eigenstate of the ^{14}N–^{13}C system, given in powers of $|C_{\mathrm{Q}}/\omega^{\mathrm{N}}_0|$ through

$$|n,m\rangle = |n,m\rangle^{(0)} + |n,m\rangle^{(1)} + \cdots \tag{7}$$

Here, $|n,m\rangle^{(0)}$ is the unperturbed eigenstate with Zeeman quantum numbers n for ^{14}N and m for ^{13}C, and $\omega^{\mathrm{N}}_0 = -\gamma_{\mathrm{N}}B_0$ is the ^{14}N Larmor frequency in the static field B_0. If relaxation is neglected, the three coherence operators obey the eigenequation

$$\hat{\mathscr{H}}_{\mathrm{comm}}|n,-) = -\omega^{(n)}|n,-), \tag{8}$$

where the commutation superoperator is defined as [18,19]

$$\hat{\mathscr{H}}_{\mathrm{comm}}|A) = |[\mathscr{H},A]). \tag{9}$$

The frequencies of the three single-quantum transitions are given by second-order perturbation theory [15] as

$$\omega^{(n)} = \langle n,1/2|\mathscr{H}|n,1/2\rangle - \langle n,-1/2|\mathscr{H}|n,-1/2\rangle$$
$$= \omega_{\mathrm{C}} + \omega^{(n)}_{\mathrm{NC}}, \tag{10}$$

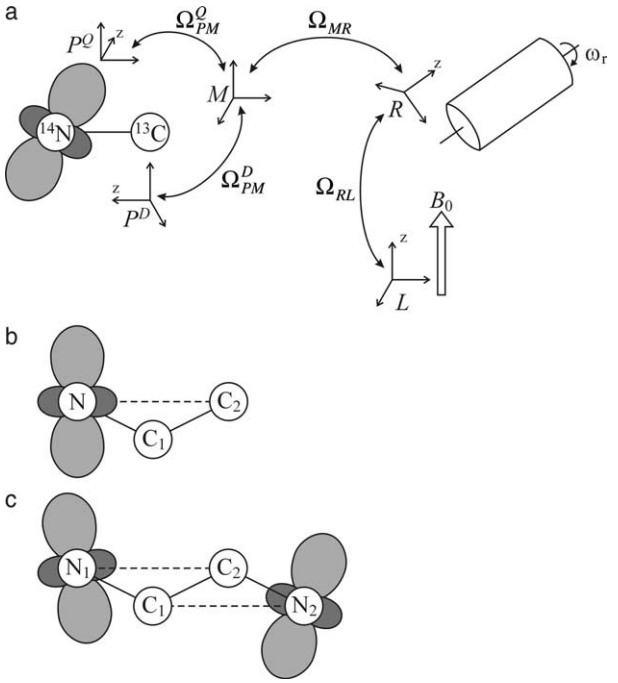

Fig. 2. (a) The relationship between the reference frames P^{D}, P^{Q}, M, R, and L. (b) A sketch of the NCC moiety in glycine, showing the numbering scheme used. C_1 and C_2 correspond to C^{α} and C', respectively. (c) A sketch of the central NCCN moiety of glycyl-glycyl-glycine, showing the numbering scheme used. C_1 and C_2 correspond to C^{α} and C' of the central glycine unit, respectively. N_1 and N_2 correspond to the nitrogens of the central and C-terminus glycine units, respectively.

where

$$\omega_{\mathrm{C}} = \omega^{\mathrm{iso}} + [A^{\mathrm{CS}}_{2,0}]^{\mathrm{L}},$$
$$\omega^{(n)}_{\mathrm{NC}} = 2n\pi J + n\sqrt{2/3}[A^{\mathrm{D}}_{2,0}]^{\mathrm{L}} + (1-(3/2)n^2)\frac{[A^{\mathrm{D}}_{2,1}]^{\mathrm{L}}[A^{\mathrm{Q}}_{2,-1}]^{\mathrm{L}} + [A^{\mathrm{D}}_{2,-1}]^{\mathrm{L}}[A^{\mathrm{Q}}_{2,1}]^{\mathrm{L}}}{\omega^{\mathrm{N}}_0}. \tag{11}$$

Here, ω^{iso} is the isotropic chemical shift of the ^{13}C spin, $[A^{\mathrm{CS}}_{2,0}]^{\mathrm{L}}$ is a component of the laboratory frame chemical shift tensor and J is the ^{13}C–^{14}N J-coupling. Terms quadratic in the dipolar or J-coupling and dipolar-J cross terms have been neglected.

In the presence of rapid MAS, it is appropriate to take the time average of Eq. (11) over the sample rotation. This neglects the MAS sideband structure and relaxation and assumes that the time-dependent perturbed states $|n,m\rangle$ are followed adiabatically as the sample rotates. This assumption is expected to be valid for spinning frequencies which are much less than the quadrupolar coupling and the Zeeman interaction. The time average coherence frequency under MAS is given by

$$\overline{\omega}^{(n)} = \omega^{\mathrm{iso}} + \overline{\omega}^{(n)}_{\mathrm{NC}}, \tag{12}$$

where

$$\overline{\omega}^{(n)}_{\mathrm{NC}} = 2\pi nJ + (1-(3/2)n^2) \times \sum_m \Big(d^2_{m,1}(\beta^{\mathrm{RL}}) d^2_{-m,-1}(\beta^{\mathrm{RL}}) + d^2_{-m,1}(\beta^{\mathrm{RL}}) d^2_{m,-1}(\beta^{\mathrm{RL}}) \Big) \frac{[A^{\mathrm{D}}_{2,m}]^{\mathrm{R}} [A^{\mathrm{Q}}_{2,-m}]^{\mathrm{R}}}{\omega^{\mathrm{N}}_0}. \quad (13)$$

Here, β^{RL} is the angle between the rotor axis and the static magnetic field, equal to $\cos^{-1}(1/\sqrt{3}) \cong 54.7°$ for exact MAS. The terms $d^2_{m,m'}(\beta)$ are reduced Wigner matrix elements [20] and the rotor frame components of the dipolar and quadrupolar Hamiltonians, $[A^{\mathrm{D}}_{2,m}]^{\mathrm{R}}$, and $[A^{\mathrm{Q}}_{2,m}]^{\mathrm{R}}$ are given by

$$[A^{\mathrm{D}}_{2,m}]^{\mathrm{R}} = \sum_{m',m''} [A^{\mathrm{D}}_{2,m''}]^{\mathrm{P}} D^2_{m'',m'}(\Omega^{\mathrm{D}}_{\mathrm{PM}}) D^2_{m',m}(\Omega_{\mathrm{MR}}),$$
$$[A^{\mathrm{Q}}_{2,m}]^{\mathrm{R}} = \sum_{m',m''} [A^{\mathrm{Q}}_{2,m''}]^{\mathrm{P}} D^2_{m'',m'}(\Omega^{\mathrm{Q}}_{\mathrm{PM}}) D^2_{m',m}(\Omega_{\mathrm{MR}}). \quad (14)$$

This expresses the dependence upon the Euler angles $\Omega^{\mathrm{D}}_{\mathrm{PM}} = \{\alpha^{\mathrm{D}}_{\mathrm{PM}}, \beta^{\mathrm{D}}_{\mathrm{PM}}, \gamma^{\mathrm{D}}_{\mathrm{PM}}\}$ and $\Omega^{\mathrm{Q}}_{\mathrm{PM}} = \{\alpha^{\mathrm{Q}}_{\mathrm{PM}}, \beta^{\mathrm{Q}}_{\mathrm{PM}}, \gamma^{\mathrm{Q}}_{\mathrm{PM}}\}$, which relate the interaction principal axis systems (denoted as P) with a common molecular frame (M). The Euler angles $\Omega_{\mathrm{MR}} = \{\alpha_{\mathrm{MR}}, \beta_{\mathrm{MR}}, \gamma_{\mathrm{MR}}\}$ relate the molecular frame with the rotor-fixed frame (R) and are random angles in a powder (Fig. 2a).

Eq. (13) may be used to predict the powder MAS spectra of ^{13}C spins coupled to ^{14}N and corresponds to the formulae given in previous papers [4,13–15]. Note that the coherences $|+1,-\rangle$ and $|-1,-\rangle$ are only split in frequency by the J-coupling. If the J-coupling is smaller than the residual dipolar coupling, the spectrum has the appearance of a 1:2 doublet [1–3,13,21].

2.2. Two ^{13}C coupled to one ^{14}N

In the case of two ^{13}C spins, the spin Hamiltonian is more complicated because of the existence of multiple heteronuclear interactions as well as homonuclear interactions. The spin Hamiltonian may be written as

$$\mathscr{H} = \mathscr{H}^{\mathrm{N}}_{\mathrm{Z}} + \mathscr{H}^{\mathrm{C}_1}_{\mathrm{Z}} + \mathscr{H}^{\mathrm{C}_2}_{\mathrm{Z}} + \mathscr{H}^{\mathrm{C}_1,\mathrm{C}_2}_{J} + \mathscr{H}^{\mathrm{C}_1,\mathrm{C}_2}_{\mathrm{D}} + \mathscr{H}^{\mathrm{C}_1,\mathrm{N}}_{J} + \mathscr{H}^{\mathrm{C}_1,\mathrm{N}}_{\mathrm{D}} + \mathscr{H}^{\mathrm{C}_2,\mathrm{N}}_{J} + \mathscr{H}^{\mathrm{C}_2,\mathrm{N}}_{\mathrm{D}}. \quad (15)$$

The numbering system for the ^{14}N–^{13}C–^{13}C system is shown in Fig. 2b. The homonuclear and heteronuclear terms do not commute with each other, leading to a complicated spectral behaviour in general.

Fortunately, the behaviour of the (± 2)-quantum $^{13}C_2$ coherences is still relatively simple. There are three (-2)-quantum coherences, notated $|n,-,-\rangle$, and defined by

$$|n,-,-\rangle = |n,-1/2,-1/2\rangle\langle n,+1/2,+1/2|, \quad (16)$$

where $|n,m_1,m_2\rangle$ is the perturbed Zeeman eigenstate with quantum numbers n, m_1, and m_2 for the ^{14}N spin and the two ^{13}C spins. These (-2)-quantum coherences obey the following commutation relationship:

$$\hat{\mathscr{H}}_{\mathrm{comm}}|n,-,-\rangle = -\omega^{(n)}|n,-,-\rangle, \quad (17)$$

where the frequencies of the three double-quantum coherences are given by

$$\omega^{(n)} = \omega_{\mathrm{C}_1} + \omega_{\mathrm{C}_2} + \omega^{(n)}_{\mathrm{NC}_1} + \omega^{(n)}_{\mathrm{NC}_2}. \quad (18)$$

Each of the terms has the form given in Eq. (11). Averaging over the magic-angle rotation gives

$$\overline{\omega}^{(n)} = \omega^{\mathrm{iso}}_{\mathrm{C}_1} + \omega^{\mathrm{iso}}_{\mathrm{C}_2} + \overline{\omega}^{(n)}_{\mathrm{NC}_1} + \overline{\omega}^{(n)}_{\mathrm{NC}_2}, \quad (19)$$

where the individual coupling terms are specified in Eq. (13). Note the absence of the homonuclear couplings in this expression. The form of the spectrum is again a 1:2 doublet in the case that the ^{14}N–^{13}C J-couplings are smaller than the residual dipolar couplings. An experimental demonstration of this is given below for [$^{13}C_2$]-glycine.

2.3. Two ^{13}C coupled to two ^{14}N

In this case, the double-quantum ^{13}C spectrum has nine components, corresponding to the nine possible combinations of the quantum numbers $n_1 = \{+1,0,-1\}$ and $n_2 = \{+1,0,-1\}$ for the two ^{14}N spins. The individual coherences are notated as

$$|n_1,-,-,n_2\rangle = |n_1,-1/2,-1/2,n_2\rangle \times \langle n_1,+1/2,+1/2,n_2|, \quad (20)$$

and have a precession frequency defined by

$$\hat{\mathscr{H}}_{\mathrm{comm}}|n_1,-,-,n_2\rangle = -\omega^{(n_1,n_2)}|n_1,-,-,n_2\rangle. \quad (21)$$

Under MAS, the time average frequencies of the nine double-quantum transitions are given by

$$\overline{\omega}^{(n_1,n_2)} = \omega^{\mathrm{iso}}_{\mathrm{C}_1} + \omega^{\mathrm{iso}}_{\mathrm{C}_2} + \overline{\omega}^{(n_1)}_{\mathrm{N}_1\mathrm{C}_1} + \overline{\omega}^{(n_1)}_{\mathrm{N}_1\mathrm{C}_2} + \overline{\omega}^{(n_2)}_{\mathrm{N}_2\mathrm{C}_1} + \overline{\omega}^{(n_2)}_{\mathrm{N}_2\mathrm{C}_2}, \quad (22)$$

where each of the coupling terms has the form specified in Eq. (13). The numbering system for the NCCN system is shown in Fig. 2c. If the J-couplings are negligible and the residual dipolar couplings are of similar magnitude for the two ^{13}C sites, the double-quantum spectrum takes the form of a 1:4:4 triplet. The weakest peak of the triplet is formed by the $|0,-,-,0\rangle$ coherence. The central peak is formed by the near degenerate $\{|0,-,-,+1\rangle, |0,-,-,-1\rangle, |+1,-,-,0\rangle, |-1,-,-,0\rangle\}$ coherences. The strong outer peak of the triplet is formed by the $\{|+1,-,-,+1\rangle, |-1,-,-,-1\rangle, |+1,-,-,-1,\rangle, |-1,-,-,+1\rangle\}$ coherences.

The precise form of the spectral multiplet depends upon the relative orientations of the ^{14}N–^{13}C dipolar couplings and the quadrupolar interaction tensors of the ^{14}N nuclei. This is illustrated by the simulations in Fig. 3, which shows the powder average double-quantum spectra of an ^{14}N–^{13}C–^{13}C–^{14}N group with two

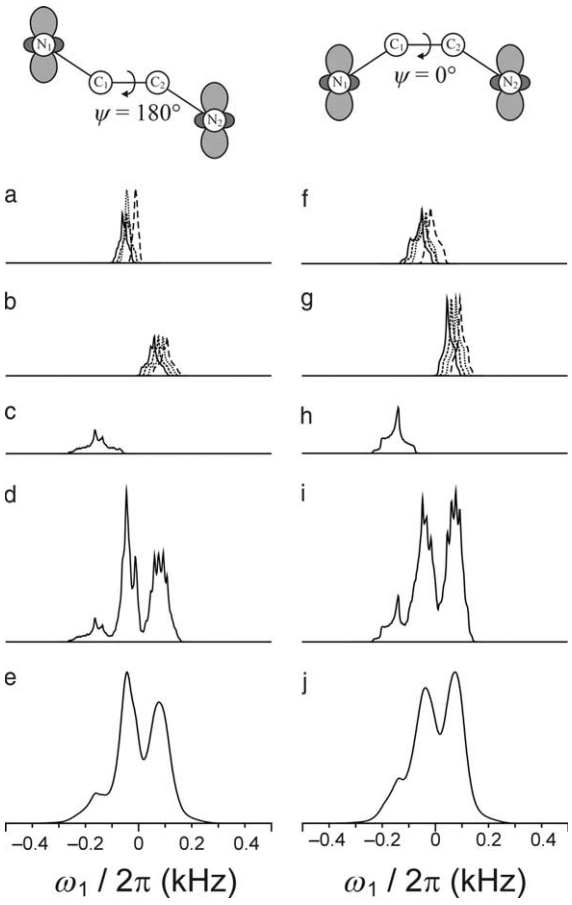

Fig. 3. The nine components of the $^{13}C_2$ double-quantum powder spectrum for two different values of (a)–(e) $\phi = \psi = 180°$, (f)–(j) $\phi = \psi = 0°$. Plots (a) and (f) show the components due to the $\{|0,-,-,+1\rangle, |0,-,-,-1\rangle, |+1,-,-,0\rangle, |-1,-,-,0\rangle\}$ coherences. Plots (b) and (g) show the components due to the $\{|+1,-,-,+1\rangle, |-1,-,-,-1\rangle, |+1,-,-,-1\rangle, |-1,-,-,+1\rangle\}$ coherences. Plots (c) and (h) show the component due to the $|0,-,-,0\rangle$ coherence. Plots (d) and (i) show the sum of the nine components. Plots (e) and (j) show the sum of the nine components with lorentzian line broadening added (full width at half height = 17 Hz). The simulation parameters were: ^{14}N quadrupolar interaction parameters $(C_Q, \eta) = (-3.01\,\text{MHz},\ 0.48)$; electric field gradient orientation as in Fig. 1b for both sites; direct dipole–dipole couplings $b_{N_1C_1}/2\pi = -791.1$ Hz, $b_{N_1C_2}/2\pi = -153.5$ Hz, $b_{N_2C_1}/2\pi = -157.5$ Hz, and $b_{N_2C_2}/2\pi = -938.1$ Hz; J-couplings $J_{N_1C_1} = 7.77$ Hz, $J_{N_1C_2} = 0$ Hz, $J_{N_2C_1} = 5.92$ Hz, and $J_{N_2C_2} = 10.55$ Hz; Larmor frequencies $\omega_0^C/2\pi = -50.372$ MHz, $\omega_0^N/2\pi = -14.471$ MHz.

different torsional angles, broken down into the nine spectral components.

If the ^{14}N–^{13}C–^{13}C–^{14}N moiety forms part of a peptide backbone, the double-quantum ^{13}C spectrum depends not only on the NCCN torsional angle ψ but also on the ϕ torsional angle of the preceding residue, since the quadrupole interaction tensors are approximately fixed with respect to the peptide planes. The "standard" orientation of the ^{14}N quadrupolar tensor with respect to the peptide plane, as determined by single crystal measurements on two dipeptides (gly-gly and gly-ala) [4], is sketched in Fig. 1b. The largest tensor component (z-axis) is approximately perpendicular to the peptide plane, while the smallest component (y-axis) is approximately along the NH bond direction, which is assumed in this paper to subtend angles of 119.4° and 118.2° with respect to the C′N and NC$^\alpha$ bonds in gly-gly-gly, respectively. If these relationships are assumed to hold exactly, while the bond lengths and bond angles are taken from crystal structures, it is possible to predict the dependence of the double-quantum spectrum on the angles ϕ and ψ.

The predicted dependence of the double-quantum $^{13}C_2$ spectrum upon ϕ and ψ for "standard" values of the quadrupole interaction tensors, molecular geometry, and electric field gradient orientations in peptides is sketched in Fig. 4. As may be seen, the predicted form of the spectrum is sometimes sensitive to the values of ϕ and ψ but a given spectral shape does not define the values of ϕ and ψ uniquely. These simulations neglect the orientational dependence of the pulse sequence used to excite the double-quantum coherence.

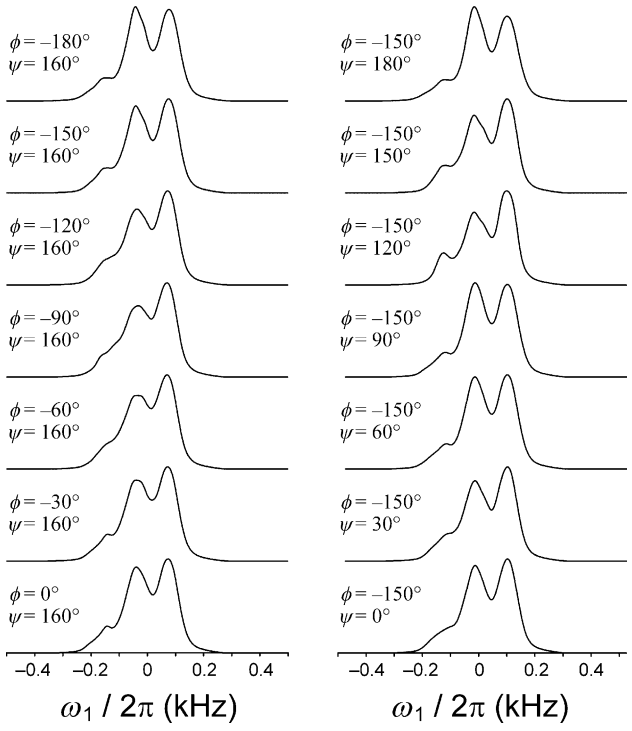

Fig. 4. Simulated $^{13}C_2$ double-quantum spectra of gly-[$^{13}C_2$]-gly-gly · HCl for a range of torsional angles at a magnetic field $B_0 = 4.7$ T. The simulation parameters are: ^{14}N quadrupolar interaction parameters $(C_Q/2\pi,\ \eta) = (-3.01\,\text{MHz},\ 0.48)$; electric field gradient orientation as in Fig. 1b for both sites; direct dipole–dipole couplings $b_{N_1C_1}/2\pi = -791.1$ Hz, $b_{N_1C_2}/2\pi = -153.5$ Hz, $b_{N_2C_1}/2\pi = -157.5$ Hz, and $b_{N_2C_2}/2\pi = -938.1$ Hz; J-couplings $J_{N_1C_1} = 7.77$ Hz, $J_{N_1C_2} = 0$ Hz, $J_{N_2C_1} = 5.92$ Hz, and $J_{N_2C_2} = 10.55$ Hz; Larmor frequencies $\omega_0^C/2\pi = -50.372$ MHz and $\omega_0^N/2\pi = -14.471$ MHz. All simulations were broadened by a Lorentzian function with full width at half height = 17 Hz.

3. Materials and methods

To acquire a double-quantum spectrum, experiments conforming to the general scheme given in Fig. 5 were used. Ramped cross-polarization [22] was used to prepare enhance ^{13}C magnetization which was converted into (± 2)-quantum coherence by an excitation sequence. The double-quantum coherences were allowed to evolve for an interval t_1 and reconverted into observable transverse magnetisation for detection. Phase cycling was used to select signals passing through (± 2)-quantum coherence.

Two different methods were used to excite and observe the ^{13}C–^{13}C double-quantum coherence (see Fig. 6). One was based upon the experiments carried out by Karlsson et al. [23,24] using pulse-assisted rotational resonance. The other was the SC14 pulse sequence developed by Brinkmann et al. [25]. In both cases the only RF irradiation during the t_1 interval was ^{1}H decoupling. The experiments were carried out on a Chemagnetics Infinity-200 spectrometer at a field of 4.7 T using 4 mm zirconia rotors.

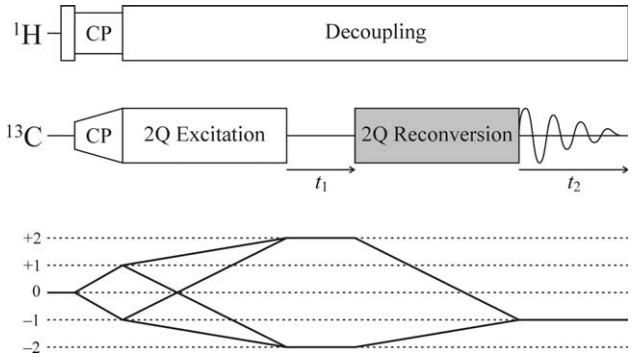

Fig. 5. General experimental scheme for the acquisition of $^{13}C_2$ double-quantum spectra and associated coherence transfer pathway diagrams. The shaded pulse sequence elements are varied in a standard four step phase cycle to select signals passing through $^{13}C_2$ double-quantum coherence.

Experiments were carried out on ^{13}C labelled samples of two different model compounds, glycine and glycyl-glycyl-glycine hydrochloride (gly-gly-gly · HCl). The glycine sample was labelled with ^{13}C in both positions in 10% of the molecules, the remaining 90% of molecules being unlabelled. To avoid the formation of polymorphs, the mixture of natural abundance glycine and labelled glycine was crystallized slowly from aqueous solution with the atmosphere exposed to a saturated NaCl solution.

The gly-gly-gly · HCl sample was prepared by solid-state synthesis and was labelled with ^{13}C in both positions on the central glycine unit in 10% of the molecules, the remaining 90% of molecules being unlabelled. The mixture of isotopomers was crystallized from a strong HCl solution. The crystal structure of gly-gly-gly · HCl has been determined by X-ray diffraction [26]. The molecule adopts an extended conformation, with torsional angles at the central glycine residue given by $\{\phi, \psi\} = \{-154.4°, +159.7°\}$.

4. Results

4.1. $^{13}C_2$-glycine

The double-quantum spectrum of [10%-$^{13}C_2$]-glycine was acquired using the scheme shown in Fig. 6a. The method is described in detail in [24]. Fig. 7a shows the full 2D spectrum of [10%-$^{13}C_2$]-glycine acquired in this manner. The experimental parameters were; spinning

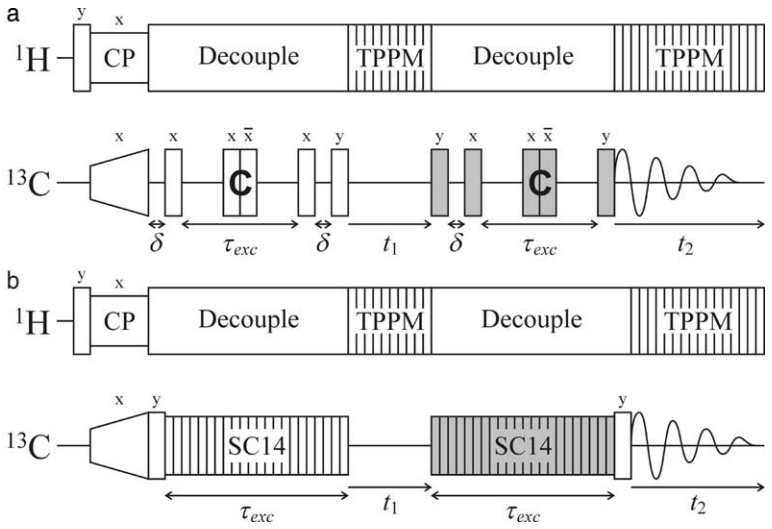

Fig. 6. Double-quantum pulse sequences used to acquire the experimental results in this paper. (a) Pulse-assisted rotational resonance (see [24]). (b) SC14 (see [25]). The shaded pulse sequence elements are varied in a standard four step phase cycle to select signals passing through $^{13}C_2$ double-quantum coherence.

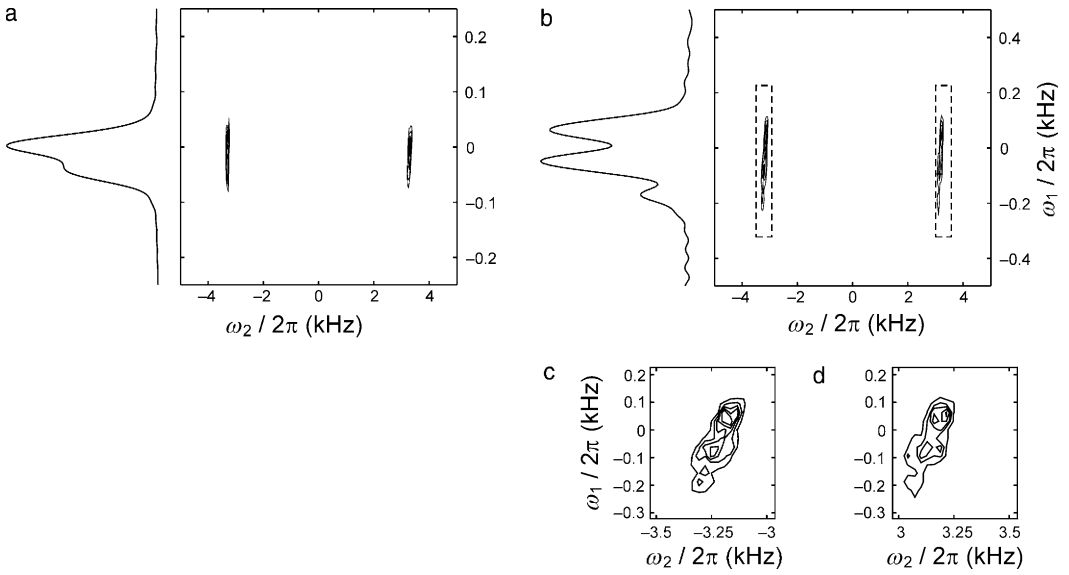

Fig. 7. (a) Experimental $^{13}C_2$ double-quantum spectrum of [10%-$^{13}C_2$]-glycine in a field of 4.7 T, obtained with the pulse sequence in Fig. 6a. The left hand peak is negative. The projection of the two-dimensional spectrum onto the ω_1 axis, with the negative left hand peak inverted in sign, is also shown. (b) $^{13}C_2$ double-quantum spectrum of gly-[10%-$^{13}C_2$]-gly-gly · HCl in a field of 4.7 T, obtained with the pulse sequence in Fig. 6b. The projection of the two-dimensional spectrum onto the ω_1-axis is also shown. (c) and (d) Expanded views of the spectral peaks in (b).

frequency $\omega_r/2\pi = 8.351$ kHz, cross-polarization contact time of 2.0 ms, $\tau_{exc} = 307\,\mu s$, $\delta = 73\,\mu s$, CW decoupling with ^1H nutation frequency of 103 kHz during excitation and reconversion, TPPM decoupling [27] during t_1 with ^1H nutation frequency of 103 kHz, pulse length of 4.6 μs and phase shift of 10°, and TPPM decoupling during t_2 with ^1H nutation frequency of 84 kHz, pulse length of 5.7 μs, and phase shift of 13°. The elements C consisted of two pulses with phases 0 and π, each of duration 29.94 μs with a nutation frequency of 38 kHz.

The pulse-assisted rotational resonance method generates a spectrum with one peak inverted in sign. Fig. 8a shows a projection of this 2D spectrum onto the ω_1-axis after sign inversion of one of the peaks. This double-quantum spectrum displays a partially resolved 1:2 doublet structure, as discussed above.

The principal values of the ^{14}N quadrupolar coupling (as well as its orientation) have been measured for glycine using single crystal ^{14}N NMR [28]. In this study, the two symmetry related molecules in the unit cell were investigated separately, leading to two different measurements of the same principal values and orientation. For both measurements, the quadrupole interaction is characterized by $C_Q = 1.182$ MHz, $\eta = 0.54$, with the V_{zz}-axis approximately along the NC bond and the V_{xx}-axis nearly perpendicular to the C–C–N plane. A simulation of this spectrum, using these interaction parameters, is shown in Fig. 8b. This simulation neglects the orientational dependence of the double-quantum excitation and reconversion processes. Nevertheless, it fits the main features of the experimental spectrum rather well.

The simulation in Fig. 8c includes the orientational dependence of the double-quantum excitation and reconversion, by weighting each component of the powder average by a function calculated as in Eqs. (10)–(26) in [24]. This orientational weighting does not have a significant effect on the simulated spectrum.

We wished to establish whether the double-quantum spectrum in Fig. 8a could be used to determine the orientation of the electric field gradient, assuming that only the principal values of the quadrupolar interaction were known. For this purpose, double-quantum spectra were simulated for a set of orientations of the electric field gradient keeping the molecular geometry fixed. The set of EFG orientations was constructed using the ZCW algorithm [29–31] and consisted of 1154 elements spanning all possible orientations. The molecular structure was taken from the published neutron diffraction study [32]. The *J*-couplings were taken from [28] and the orientational dependence of the double-quantum excitation and reconversion was taken into account based on the experimental parameters. Fig. 9 shows those EFG orientation which gave acceptable fits to the experimental spectrum, superimposed onto a representation of the CCN moiety of the glycine molecule. These 81 orientations provided simulations for which the mean square difference between the simulated and experimental spectra (χ^2) was less than $\sqrt{2}$ times the minimum value [33]. As can be seen, this group have V_{zz} components which are clustered around the C–N bond, whilst the V_{xx} and V_{yy} components are distributed roughly uniformly around the plane perpendicular to the C–N bond. Thus, the orientation of the V_{zz} component conforms with that determined by earlier experiments [28].

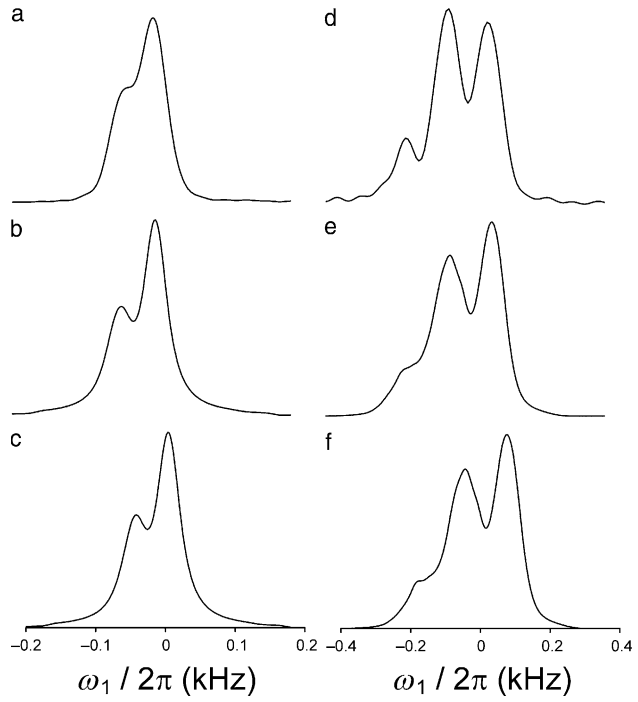

Fig. 8. (a) $^{13}C_2$ double-quantum spectrum of [10%-$^{13}C_2$]-glycine in a field of 4.7 T. (b) Simulation using the following parameters: direct dipole–dipole couplings $b_{NC_1}/2\pi = -660$ Hz, $b_{NC_2}/2\pi = -138$ Hz, $b_{C_1C_2}/2\pi = -2084.3$ Hz, C_1–C_2–N angle of 111.8°, J-couplings $J_{NC_1} = 4.5$ Hz, $J_{NC_2} = 0$ Hz, $C_Q = 1.182$ MHz, $\eta = 0.54$, electric field gradients oriented with V_{zz} along the N–C bond and V_{xx} perpendicular to the N–C–C plane, lorentzian line broadening with full width at half height = 17 Hz. (c) Simulation using the same parameters as (b) but taking into account the double-quantum excitation and reconversion efficiency. (d) $^{13}C_2$ double-quantum spectrum of gly-[10%-$^{13}C_2$]-gly-gly · HCl in a field of 4.7 T. (e) Simulation using the following parameters: ^{14}N quadrupolar interaction parameters for both sites $(C_Q, \eta) = (-3.01\,\text{MHz}, 0.48)$; Electric field gradients orientated with V_{zz} perpendicular to the peptide bond plane and V_{yy} parallel to the N–H bond; Direct dipole–dipole couplings $b_{N_1C_1}/2\pi = -791.1$ Hz, $b_{N_1C_2}/2\pi = -153.5$ Hz, $b_{N_2C_1}/2\pi = -157.5$ Hz, and $b_{N_2C_2}/2\pi = -938.1$ Hz; J-couplings $J_{N_1C_1} = 7.77$ Hz, $J_{N_1C_2} = 0$ Hz, $J_{N_2C_1} = 5.92$ Hz, and $J_{N_2C_2} = 10.55$ Hz; torsional angles $\phi = -153°$, and $\psi = -160°$; Larmor frequencies $\omega_0^C/2\pi = -50.372$ MHz, $\omega_0^N/2\pi = -14.471$ MHz, Lorentzian line broadening with full width at half height = 17 Hz. (f) Simulation using the same parameters as (e) but taking into account the double-quantum excitation and reconversion efficiency.

The present study gives no information as to the orientation of the V_{xx} and V_{yy} components. This is because the EFG tensor has a low asymmetry parameter and the C_2–N coupling is relatively weak.

4.2. Glycyl-[$^{13}C_2$]-glycyl-glycine

The double-quantum spectrum of gly-[10%-$^{13}C_2$]-gly-gly was acquired using the scheme shown in Fig. 6b. The SC14 pulse sequence is a supercycled version of the $C14_4^5$ pulse sequence, as described in [25]. Fig. 7b shows the full 2D spectrum of gly-[10%-$^{13}C_2$]-gly-gly acquired in this manner. Figs. 7c and d provide expanded views of

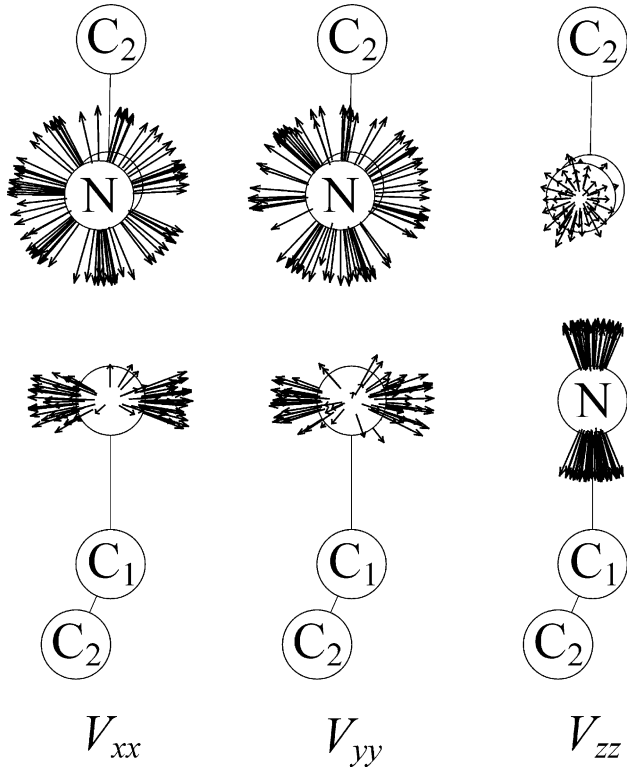

Fig. 9. Ensemble of principal axis directions of the ^{14}N electric field gradient in glycine giving an acceptable fit to the experimental spectrum. The atoms are labelled as in Fig. 2b. The two rows show the molecule viewed from two different directions.

the major peaks. The tilted appearance of these peaks arises because the residual dipolar shifts of the single-quantum and double-quantum coherences are in the same sense. The experimental parameters were; spinning frequency $\omega_r/2\pi = 11.0$ kHz, cross-polarization contact time of 2.0 ms, $\tau_{exc} = 727$ μs, CW decoupling during excitation and reconversion with ^1H nutation frequency of 109 kHz, TPPM decoupling during t_1 with ^1H nutation frequency of 109 kHz, pulse length of 4.6 μs and phase shift of 15°, and TPPM decoupling during t_2 with ^1H nutation frequency of 85 kHz, pulse length of 5.9 μs and phase shift of 9°. Fig. 8d shows a projection of this 2D spectrum onto the ω_1-axis.

The crystal structure of gly-gly-gly · HCl is known [26], but information on the quadrupolar interaction tensor is incomplete. An NQR study of gly-gly-gly (not the hydrochloride) [34] gives values of $(C_Q, \eta) = (-3.01\,\text{MHz}, 0.48)$ and $(-3.08\,\text{MHz}, 0.76)$ for the central and C-terminal ^{14}N sites, respectively. The orientations of the electric field gradient may be guessed from the single crystal studies of gly-gly and gly-ala [4]. A simulation based on the X-ray structure [26], the known J-couplings [35], the quadrupolar interaction principal values of gly-gly-gly and the "standard" quadrupolar interaction parameters is shown in Fig. 8e. As may be seen, the general features of the double-quantum spectrum are reproduced but the amplitudes of the peaks are

not in agreement with experiment. If the double-quantum orientational dependence is taken into account, as discussed in Ref. [25], then the form of the spectrum does not change significantly (Fig. 8f).

The match of the simulation with experiment cannot be improved significantly by adjusting the principal values of the quadrupole interaction tensors. Fig. 10a shows a simulation in which the two quadrupolar interaction tensors take their "standard" orientations V_{zz} perpendicular to the peptide plane, V_{yy} along the N–H bond) but with the principal values set to the same value, $(C_Q, \eta) = (-3.01\ \text{MHz}, 0.48)$. The simulation shown at the right hand side is still not a quantitative match with the experimental spectrum.

The match with experiment is improved significantly if the orientation of one of the electric field gradient tensors is rotated around its own x-axis by about 51° (Fig. 10b). The positions and amplitudes of the double-quantum peaks are now in good agreement with the experimental spectrum (Fig. 10c).

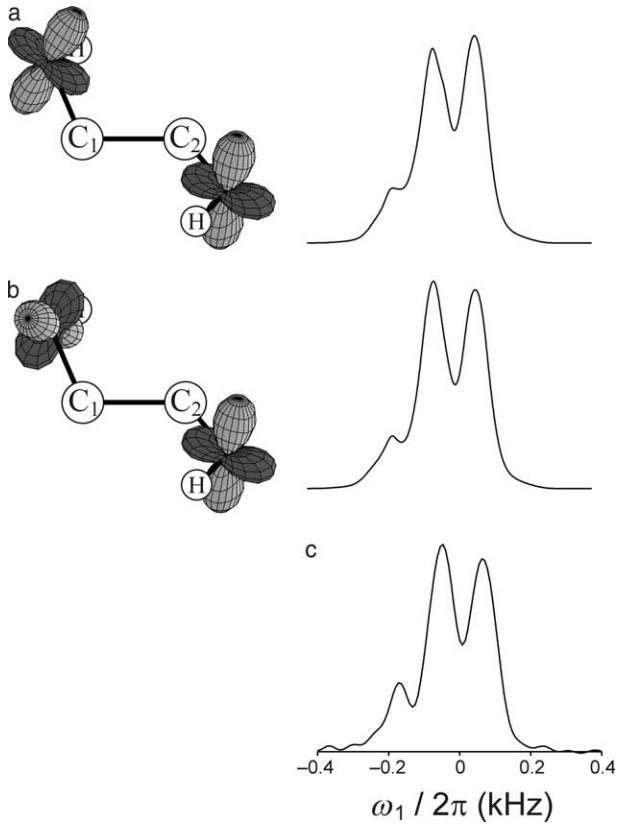

Fig. 10. (a) Graphical representation of the ^{14}N electric field gradients for the ^{14}N nuclei flanking the central glycine residue in gly-gly-gly and a simulation of the $^{13}C_2$ double-quantum spectrum of gly-[10%-$^{13}C_2$]-gly-gly. The quadrupolar interaction tensors for both ^{14}N nuclei have principal values defined by $(C_Q, \eta) = (-3.01\,\text{MHz}, 0.48)$, with the principal axes oriented as in Fig. 1b. (b) Graphical representation and corresponding simulation in the case that the EFG tensor of the N_1 site is rotated by the Euler angles $\{\alpha_1^Q, \beta_1^Q, \gamma_1^Q\} = \{91.7°, 51.0°, 56.8°\}$ from the orientation shown in Fig. 1b. (c) Experimental double-quantum spectrum of gly-[10 %-$^{13}C_2$]-gly-gly · HCl.

Unfortunately it is not possible to deduce the orientations and magnitudes of the quadrupolar interaction parameters uniquely from this projection of a single double-quantum spectrum. There are too many parameter sets which provide an equally good fit to the experimental data. More information is likely to be provided by a combination of double-quantum spectra with single-quantum spectra or simulations of the full two-dimensional peaks shown in Figs. 7c and d.

Fig. 11 shows the χ^2 values of the fit of simulations to the gly-gly-gly · HCl double-quantum spectrum as a function of the two torsional angles, ϕ and ψ, taken in steps of 10°. The plot shows the expected symmetry that $\chi^2(\phi, \psi) = \chi^2(-\phi, -\psi)$. The lowest contour is at a level corresponding to $\sqrt{2}$ times the minimum value of χ^2, so that all of the black areas correspond to acceptable fits. The simulations used for this plot use the same "standard" orientations and magnitudes for the principal components of the EFG tensors as were used for the simulation shown in Fig. 10a. The orientational dependence of the double-quantum excitation and reconversion is also included. The known torsional angles obtained from X-ray diffraction correspond to the white triangle, which lies just outside a region of acceptable fit. As mentioned above, this indicates that the principal values and/or the principal axes of the quadrupolar tensors are in error but, at this point, we are unable to assign a corrected set of tensor components in a unique way.

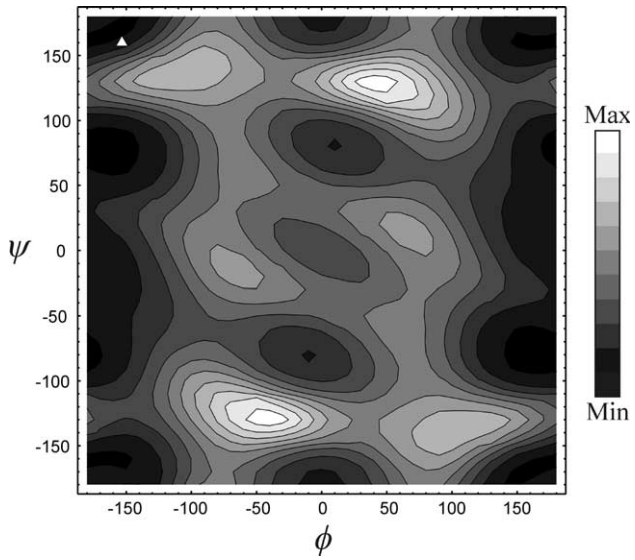

Fig. 11. Mean square difference between experiment and simulation (χ^2) for the experimental spectrum of gly-[10%-$^{13}C_2$]-gly-gly · HCl, as a function of the torsional angles (ϕ, ψ) of the central glycine residue. The standard orientations of the electric field gradients, depicted in Fig. 4, were used. The lowest contour corresponds to a level equal to $\sqrt{2}$ times the minimum value of χ^2. The torsional angles determined by X-ray diffraction are represented by a white triangle. The simulation parameters for this plot are the same as in Fig. 4.

5. Conclusions

We have examined the $^{13}C_2$ double-quantum spectra of powdered materials in which the $^{13}C_2$ pair is coupled to one or two ^{14}N nuclei. In [10%-$^{13}C_2$]-glycine, the $^{13}C_2$ pair is coupled to a single ^{14}N nucleus, to a good approximation. The double-quantum spectrum has the form of a 1:2 doublet, as predicted. The spectrum is sensitive to the orientation of the largest component of the ^{14}N quadrupolar interaction, enabling an estimation of the corresponding principal axis direction in agreement with previous single crystal studies.

In gly-[10%-$^{13}C_2$]-gly-gly · HCl, the $^{13}C_2$ pair is coupled to two ^{14}N nuclei. The double-quantum spectrum has the form of a 1:4:4 triplet, as predicted. However, the quantitative form of the spectrum is not entirely in agreement with simulations employing principal values of the quadrupolar interactions obtained from measurements on gly-gly-gly, together with standard orientations of the EFG tensors with respect to the peptide planes. We are able to achieve a good match between experiment and simulation by adjusting the quadrupolar interaction parameters, but we are unable to define the revised parameters uniquely, since there are too many possibilities. Nevertheless, the double-quantum experiment described here is a sensitive test of the validity of assumed electric field gradient orientations. It is not, at the moment, a feasible way of determining torsional angles unambiguously.

There are a number of restrictions upon the application of the experiment. First, glycine residues present a favourable case since there are no side chains. In general, ^{13}C nuclei in the amino acid side chains will complicate the appearance of the $^{13}C_2$ double-quantum spectrum through the participation of homonuclear *J*-couplings and dipole–dipole couplings. Second, experiments described in this paper are difficult to perform at high magnetic field, since the second-order dipolar shifts are inversely proportional to the Larmor frequency. It is possible to employ similar effects in high magnetic field by using RF fields to recouple the ^{14}N spins (e.g., REDOR, REAPDOR, and TRAPDOR), for example by irradiating the overtone transition [36,37].

Acknowledgments

This research was supported by the Göran Gustafsson Foundation for Research in the Natural Sciences and Medicine, and the Swedish Natural Science Foundation. We thank O.G. Johannessen and A. Brinkmann for experimental help. C.E.H. is the recipient of a Marie Curie Individual Fellowship (HPMF-CT-1999-00199) from the European Union.

References

[1] S.J. Opella, M.H. Frey, T.A. Cross, Detection of individual carbon resonances in solid proteins, J. Am. Chem. Soc. 101 (1979) 5856–5857.
[2] C.L. Groombridge, R.K. Harris, K.J. Packer, B.J. Say, S.F. Tanner, High-resolution ^{13}C NMR spectra of solid nitrogen-containing compounds, J. Chem. Soc. Chem. Commun. 4 (1980) 174–175.
[3] M.H. Frey, S.J. Opella, High-resolution features of the ^{13}C NMR spectra of solid amino acids and peptides, J. Chem. Soc. Chem. Commun. 11 (1980) 474–475.
[4] A. Naito, S. Ganapathy, C.A. McDowell, ^{14}N quadrupole effects in CP-MAS ^{13}C NMR spectra of organic compounds in the solid state, J. Magn. Reson. 48 (1982) 367–381.
[5] X. Feng, Y.K. Lee, D. Sandström, M. Edén, H. Maisel, A. Sebald, M.H. Levitt, Direct determination of a molecular torsional angle by solid-state NMR, Chem. Phys. Lett. 257 (1996) 314–320.
[6] S. Ravindranathan, X. Feng, T. Karlsson, G. Widmalm, M.H. Levitt, Investigation of carbohydrate conformation in solution and in powders by double-quantum NMR, J. Am. Chem. Soc. 122 (2000) 1102–1115.
[7] S. Ravindranathan, T. Karlsson, K. Lycknert, G. Widmalm, M.H. Levitt, Conformation of the glycosidic linkage in a disaccharide investigated by double-quantum solid-state NMR, J. Magn. Reson. 151 (2001) 136–141.
[8] X. Feng, P.J.E. Verdegem, Y.K. Lee, D. Sandström, M. Edén, P.H.M. Bovee-Guerts, W.J. de Grip, J. Lugtenburg, H.J.M. de Groot, M.H. Levitt, Direct determination of a molecular torsional angle in the membrane protein rhodopsin by solid-state NMR, J. Am. Chem. Soc. 119 (1997) 6853–6857.
[9] X. Feng, P.J.E. Verdegem, M. Edén, D. Sandström, Y.K. Lee, P.H.M. Bovee-Guerts, W.J. de Grip, J. Lugtenburg, H.J.M. de Groot, M.H. Levitt, Determination of a molecular torsional angle in the metarhodopsin-I photointermediate of bovine rhodopsin by double-quantum solid-state NMR, J. Biomol. NMR 16 (2000) 1–8.
[10] J.C. Lansing, M. Hohwy, C.P. Jaroniec, A.F.L. Creemers, J. Lugtenburg, J. Herzfeld, R.G. Griffin, Chromophore distortions in the bacteriorhodopsin photocycle: evolution of the H–C14–C15–H dihedral angle measured by solid-state NMR, Biochemistry 41 (2002) 431–438.
[11] X. Feng, M. Edén, A. Brinkmann, H. Luthman, L. Eriksson, A. Gräslund, O.N. Antzutkin, M.H. Levitt, Direct determination of a peptide torsional angle by solid-state NMR, J. Am. Chem. Soc. 119 (1997) 12006–12007.
[12] P.R. Costa, J.D. Gross, M. Hong, R.G. Griffin, Solid-state NMR measurement of ψ in peptides: a NCCN 2Q-heteronuclear local field experiment, Chem. Phys. Lett. 280 (1997) 95–103.
[13] A. Naito, S. Ganapathy, C.A. McDowell, High resolution solid state ^{13}C NMR spectra of carbons bonded to nitrogen in a sample spinning at the magic angle, J. Chem. Phys. 74 (1981) 5393–5397.
[14] J.G. Hexem, M.H. Frey, S.J. Opella, Molecular and structural information from ^{14}N–^{13}C dipolar couplings manifested in high resolution ^{13}C NMR spectra of solids, J. Chem. Phys. 77 (1982) 3847–3856.
[15] A.C. Olivieri, L. Frydman, L.E. Diaz, A simple approach for relating molecular and structural information to the dipolar coupling ^{13}C–^{14}N in CPMAS NMR, J. Magn. Reson. 75 (1987) 50–62.
[16] M. Mehring, Internal spin interactions & rotations in solids, In: Encyclopedia of Nuclear Magnetic Resonance, Wiley, Chichester, 1996, pp. 2585–2603.

[17] A.J. Vega, Quadrupolar nuclei in solids, In: Encyclopedia of Nuclear Magnetic Resonance, Wiley, Chichester, 1996, pp. 3869–3889.
[18] J. Jeener, Superoperators in magnetic resonance, Adv. Magn. Reson. 10 (1982) 1–51.
[19] M. Mehring, V.A. Weberruss, Object-Oriented Magnetic Resonance, Academic Press, New York, 2001.
[20] D.A. Varshalovich, A.N. Moskalev, V.K. Khersonkii, Quantum Theory of Angular Momentum, World Scientific, Singapore, 1988.
[21] J.G. Hexem, M.H. Frey, S.J. Opella, Influence of ^{14}N on ^{13}C NMR spectra of solids, J. Am. Chem. Soc. 103 (1981) 224–228.
[22] G. Metz, X.L. Wu, S.O. Smith, Ramped-amplitude cross-polarization in magic-angle-spinning NMR, J. Magn. Reson. A 110 (1994) 219–227.
[23] T. Karlsson, M. Edén, H. Luthman, M.H. Levitt, Efficient double-quantum excitation in rotational resonance NMR, J. Magn. Reson. 145 (2000) 95–107.
[24] T. Karlsson, C.E. Hughes, J. Schmedt auf der Günne, M.H. Levitt, Double-Quantum excitation in the NMR of spinning solids by pulse-assisted rotational resonance, J. Magn. Reson. 148 (2001) 238–247.
[25] A. Brinkmann, M. Edén, M.H. Levitt, Synchronous helical pulse sequences in magic-angle spinning NMR. Double quantum recoupling of multiple-spin systems, J. Chem. Phys. 112 (2000) 8539–8554.
[26] V. Lalitha, E. Subramanian, Glycyl-glycyl-glycine hydrochloride, $C_6H_{11}N_3O_4 \cdot HCl$, Cryst. Struct. Commun. 11 (1982) 561–564.
[27] A.E. Bennett, C.M. Rienstra, M. Auger, K.V. Lakshmi, R.G. Griffin, Heteronuclear decoupling in rotating solids, J. Chem. Phys. 103 (1995) 6951–6958.
[28] R.A. Haberkorn, R.E. Stark, H. van Willigen, R.G. Griffin, Determination of bond distances and bond angles by solid-state nuclear magnetic resonance ^{13}C and ^{14}N NMR study of glycine, J. Am. Chem. Soc. 103 (1981) 2534–2539.
[29] S.K. Zaremba, Good lattice points, discrepancy, and numerical integration, Ann. Mat. Pura Appl. 73 (1966) 293–317.
[30] H. Conroy, Molecular Schrödinger equation. VIII. A new method for the evaluation of multidimensional integrals, J. Chem. Phys. 47 (1967) 5307–5318.
[31] V.B. Cheng, H.H. Suzukawa, M. Wolfsberg, Investigations of a nonrandom numerical method for multidimensional integration, J. Chem. Phys. 59 (1973) 3992–3999.
[32] P.-G. Jönsson, Å. Kvick, Precision neutron diffraction structure determination of protein and nucleic acid components. III. The crystal and molecular structure of the amino acid α-glycine, Acta Cryst. B 28 (1972) 1827–1833.
[33] W.H. Press, B.P. Flannery, S.A. Teukolsky, W.T. Vetterling, Numerical Recipes, Cambridge University Press, Cambridge, MA, 1986.
[34] D.T. Edmonds, P.A. Speight, Nitrogen quadrupole resonance in amino acids, Phys. Lett. 34A (1971) 325–326.
[35] F. Delaglio, D.A. Torchia, A. Bax, Measurement of nitrogen-15 carbon-13 J couplings in Staphylococcal nuclease, J. Biomol. NMR 1 (1991) 439–446.
[36] S.S. Wi, L. Frydman, Heteronuclear recoupling in solid-state magic-angle-spinning NMR via overtone irradiation, J. Am. Chem. Soc. 123 (2001) 10354–10361.
[37] K. Takegoshi, T. Yano, K. Takeda, T. Terao, Indirect high-resolution observation of N-14 NMR in rotating solids, J. Am. Chem. Soc. 123 (2001) 10786–10787.